small methods
www.small-methods.com

High Chemical Potential Driven Amorphization of Pd-based Nanoalloys

Qiaorong Jiang, Yongdi Dong, Linzhe Lü, Zhiping Zheng, Zi-Ang Nan, Jinyu Ye, Haixin Lin, Zhiyuan Jiang, and Zhaoxiong Xie**

Amorphous metals and alloys are promising candidates for superior catalysts in many catalytic and electrocatalytic reactions. It is of great urgency to develop a general method to construct amorphous alloys and further clarify the growth mechanism in a wet-chemical system. Herein, inspired by the conservation of energy during the crystallization process, amorphous PdCu nanoalloys have been successfully synthesized by promoting the chemical potential of the building blocks in solution. Benefiting from the abundant active sites and enhanced corrosion resistance, the synthesized amorphous PdCu nanostructures exhibit superior catalytic activity and durability over the face-centered cubic one in formic acid decomposition reaction. More importantly, the successful fabrications of amorphous PdFe, PdCo, and PdNi further demonstrate the universality of the above strategy. This proposed strategy is promising to diversify the amorphous family.

1. Introduction

Just as morphology, size, and surface structure, the bulk structure of metal nanomaterials is also a key factor to determine their physicochemical properties.[1] Compare with face-centered cubic (*fcc*), hexagonal close-packed, body-centered cubic, and other common 3D long-range ordered phase structures, amorphous structure, a thermodynamic metastable phase with high inner energy,[2] is one special disordered phase with lack of long-range translation operation.[3] Amorphous metal materials have intriguing properties for promising applications due to their unique disordered atomic arrangement.[2,4] For instance, owing to the isotropy in chemical composition and geometric configuration, the lack or even absence of domain boundaries endows amorphous materials with high resistance to corrosion in both acidic and alkaline conditions, which is conducive to improve the stability of related materials.[5] More importantly, benefiting from the flexible interaction between neighboring atoms, the metallic bonds of the amorphous one can be deformed or twisted compared with the crystalline counterparts, resulting in far more amount of coordination unsaturated sites, which can act as active sites to improve catalytic activity.[6] Therefore, fabricating more functional amorphous alloys to meet the demands of practical application is of great interest. Apart from general mechanical amorphization from the crystalline counterparts,[7] several chemical methods have been developed to prepare amorphous metal-based materials recently.[6e,8] However, most of the current syntheses still rely on inefficient trial-and-error processes. A rational synthesis strategy for amorphous metals based on deep mechanism consideration of crystal growth process is highly demanded.

In the process of fast nucleation, the energy dispersion in this short time can be almost ignored, therefore, this system can be regarded as an infinitely close to adiabatic system. In fact, in an ideal adiabatic system,[9] according to the energy conservation during the crystallization process, the variation of Gibbs free energy (dG) can be expressed by Equation 1 (see Supporting Information S1 for details)

$$dG = \left(\mu_l - \mu_s\right)\, dn_l + \sigma dS = 0 \tag{1}$$

For the solid with specific bulk structure, μ_s can be considered as a constant. Accordingly, the excessive energy for transforming the building block into solid should be transferred to the surface energy of solid (σdS), it has been reported that high μ_l leads to the formation of crystal exposed with high surface energy facets.[10] On the other hand, generally, the final phase structure of the nanocrystals are determined by the structure of the nuclei.[11] Considering the nucleation stage, the nuclei are of near-sphere morphology with similar small size, hence, the difference of σdS is quite small and can be ignored, thus it can be speculated that μ_l should affect μ_s by changing the phase

Q. Jiang, Y. Dong, L. Lü, Z. Zheng, Z.-A. Nan, H. Lin, Z. Jiang, Z. Xie
Department of Chemistry, State Key Laboratory of Physical Chemistry of Solid Surface, College of Chemistry and Chemical Engineering
Xiamen University
Xiamen, Fujian 361005, P. R. China
E-mail: haixinlin@xmu.edu.cn; zxxie@xmu.edu.cn
J. Ye
Testing and Analysis Center, College of Chemistry and Chemical Engineering
Xiamen University
Xiamen, Fujian 361005, P. R. China
H. Lin, Z. Xie
Innovation Laboratory for Sciences and Technologies of Energy Materials of Fujian Province (IKKEM)
Xiamen, Fujian 361005, P. R. China

The ORCID identification number(s) for the author(s) of this article can be found under https://doi.org/10.1002/smtd.202201513

DOI: 10.1002/smtd.202201513

structures of solid, high μ_l could increase the chemical potential of nanoparticles and produce metastable structures (with high μ_s), while low μ_l results in low energy state products (with low μ_s). Very recently, we found that by varying the chemical potential of growth units during the nucleation process, the evolution from cyclic penta-twinned to single-crystalline Pt nanostructures can be controlled.[12] Herein, we propose that the amorphous structures with high $\mu_s$can also be precisely controlled by governing high μ_l in the nucleation process based on the similar consideration. PdCu alloy was first adopted as a typical example to verify the correctness of the above strategy. The universality of this strategy was then proved with the successful synthesis of PdFe, PdCo, and PdNi amorphous nanoparticles.

2. Results and Discussion

2.1. Growth Mechanism

For the growth of metal nanoparticles via wet-chemical methods, the metal precursor should be first reduced to metal atoms, and then the atoms gather and nucleate. The nucleation can be described as the following two steps:

$$M^{n+}\,(\text{solution}) + ne^- \xrightarrow{r} M^0\,(\text{solution}, \mu_l)\ (\text{Reduction step}) \quad (2)$$

$$M^0\,(\text{solution}, \mu_l) \xrightarrow{\Delta\mu} M\,(\text{solid}, \mu_s)\ \ (\text{Nucleation step}) \quad (3)$$

It is clear that μ_s can be directly affected by μ_l, determined by the instantaneous concentration of metal atoms (see Supporting Information S2 for details), which is closely related to the reduction reaction rate. Preciously control the μ_l is the key factor to governing the μ_s of the final products. After thorough analysis of the above two steps, we hypothesized that controllable tuning of μ_l can be effectively realized by the following methods. In the process of reduction step, for the same volume of reaction solution and same amount of precursor, increasing the concentration of reductant is undoubtedly one of the most effective methods to increase the reduction rate and then elevate μ_l. We proposed that there are two ways to control the concentration of reductant. First, adding larger amount of reductant at once can greatly increase the initial concentration of reductant, which is critical to the μ_l for nucleation. Second, the concentration of reductant will decrease over time, so the adding speed of reductant will restrict the highest reductant concentration that can be reached during the whole process. In addition, when focus on the nucleation step, even for the systems with the same metal atoms production rate, the different dispersion states of metal atoms will directly determine the μ_l. The local concentration of the newly formed metal atoms and μ_l will decrease if the atoms can be rapidly and uniformly dispersed at the moment of formation. On the contrary, if the diffusion is inhibited and the local concentration increases, the local μ_l will effectively increase. On the basis of the above, three most effective methods, including varying the amount and the adding speed of reductant, and the stirring rate (**Figure 1**), were then adopted to control the phase structure of product through tuning μ_l during the nucleation step.

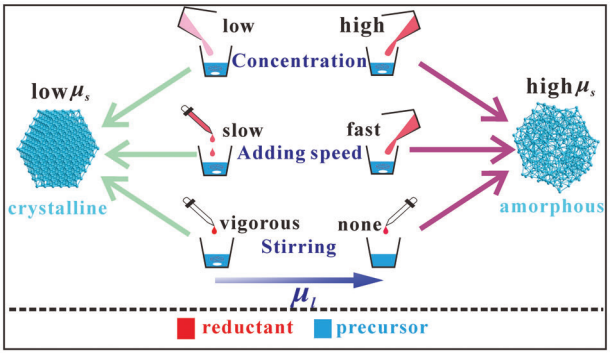

Figure 1. Schematic illustration of the chemical potential dependent phase structure control via three methods.

2.1.1. Amount Control

In the first case, when a dilute $NaBH_4$ solution (0.15 mmol, 10 mL) was poured into the precursor solution, the synthesized PdCu nanoalloys are typical *fcc* structure (**Figure 2**a) with irregular shapes and the main size is about 5–15 nm (Figure 2b, Figure S1a, Supporting Information). Selected area electron diffraction (SAED) pattern and high resolution transmission electron microscope (HRTEM) image were then collected to further clarify the local structures of the products. Considering the inherent tiny size of the products, SAED pattern (Figure 2b inset) still exhibits four distinct diffraction rings, indicating a good crystallinity of PdCu nanoalloys. The crystal lattice viewed from [001] direction is composed of two groups of fringes with the same d-space of 1.9 Å and a cross angle of 90°, which correspond to the (200) planes of PdCu alloys (Figure 2c). The chemical composition of these nanoparticles was investigated using high-angle annular dark field scannnig transmission elecreon microscope (HAADF-STEM) coupled with energy dispersive X-ray spectroscopy (EDX) and inductively coupled plasma optical emission spectrometry (ICP-OES). Both elemental mappings and line profiles indicate that the product is composed of uniformly distributed Pd and Cu elements, and ICP-OES indicates the molar ratio of Cu:Pd = 49.7:50.3 (Table S1, Supporting Information). According to the results above, the crystalline PdCu nanoalloys (named as PdCu-cryst) were successfully synthesized via the facile reduction method.

Afterward, when fix the volume of the reaction solution, with larger amount of $NaBH_4$, the crystallinity of the products decreases (Figure S2, Supporting Information), and the phase structure of the final products is even extremely different when the adding amount of $NaBH_4$ is up to 1.5 mmol. Figure 2d is a typical PXRD pattern of amorphous phase, only presenting a strong and broad prominent peak at about 42° (2θ) and another weaker and broader peak at about 75°. Besides, the other diffraction peaks (such as (200) (311), et al.) are vanished, suggesting weak long-range correlation. This PXRD pattern clearly presents the amorphous features of the synthesized products (named as PdCu-amor). In addition, local structure and morphology were then investigated by TEM. As is shown that the size and morphology of the nanoparticles are quite similar to which of PdCu-cryst (Figure 2e, Figure S1d, Supporting Information). The corresponding SAED pattern exhibits only two diffuse halos

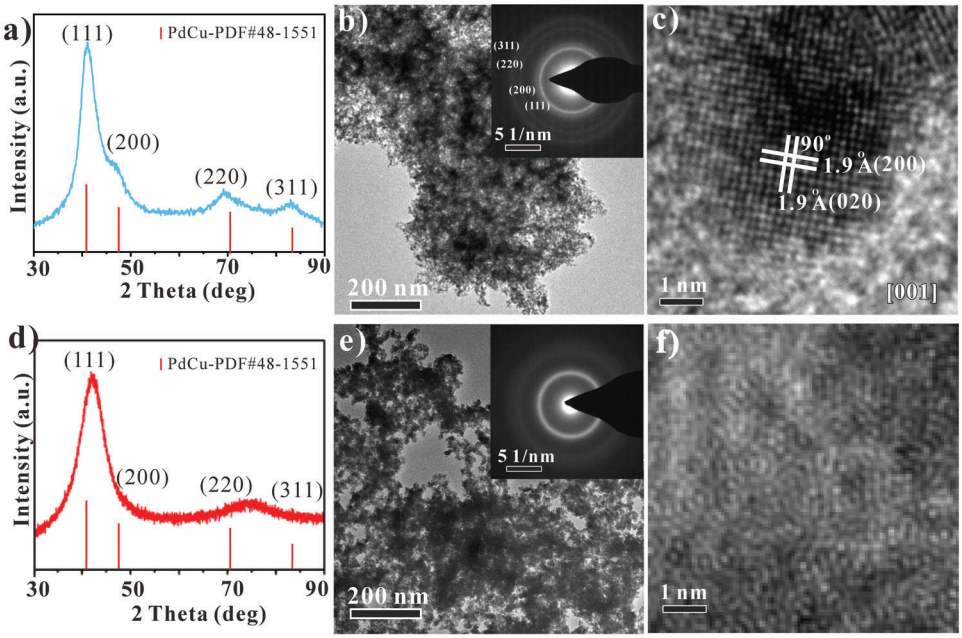

Figure 2. Typical structure features and morphology of the synthesized PdCu nanoalloys by pouring 10 mL $NaBH_4$ solution into 30 mL precursor solution. a) PXRD pattern, b) TEM image at low magnification (inset: corresponding SAED pattern), and c) HRTEM image of the PdCu nanoalloys with 0.15 mmol $NaBH_4$; d) PXRD pattern, e) TEM image at low magnification (inset: SAED pattern), and f) HRTEM image of the PdCu nanoalloys with 1.5 mmol $NaBH_4$.

(Figure 2e inset), which consists well with the PXRD pattern, and no obvious periodic lattice but only random stacked structures can be observed in HRTEM image (Figure 2f). Both SAED pattern and HRTEM image illustrate the barely crystalline feature of the amorphous phase. HAADF-STEM and the coupled EDX further prove that the synthesized amorphous nanoparticles are homogeneously alloyed, and the molar ratio of Cu:Pd = 49.5:50.5 (Table S1, Supporting Information), close to which of PdCu-cryst. This phase variation confirms that increasing the amount of the reductant is helpful to elevate the μ_s of the final products.

2.1.2. Adding Speed Control

The amount of reductant is not the decisive key factor in the formation of amorphous phase. In the concentrated condition, the reduction rate can be further governed by the adding speed of the reductant solution and then affect the phase of the final products. Hence, In the second case, instead of the one-time pouring method, when adding the concentrated $NaBH_4$ solution into the precursor solution dropwise, the main products inclined to present standard *fcc* features (**Figure 3**a) with the molar ratio of Cu:Pd = 50.6:49.4 (Table S1, Supporting Information). The TEM image further illustrates that the main product is also about 5–15 nm in size (Figure S3, Supporting Information), and the four distinct diffraction rings are the typical diffraction signs of polycrystals of *fcc* structure (Figure 3b). The main reason is as follows: during the whole reduction process, the reductant will be continuously consumed, while the adding speed is much slower than the consumption speed, which can efficiently prevent the accumulation of reductant although the adding amount is increasing, then the concentration of the generated fresh metal atoms

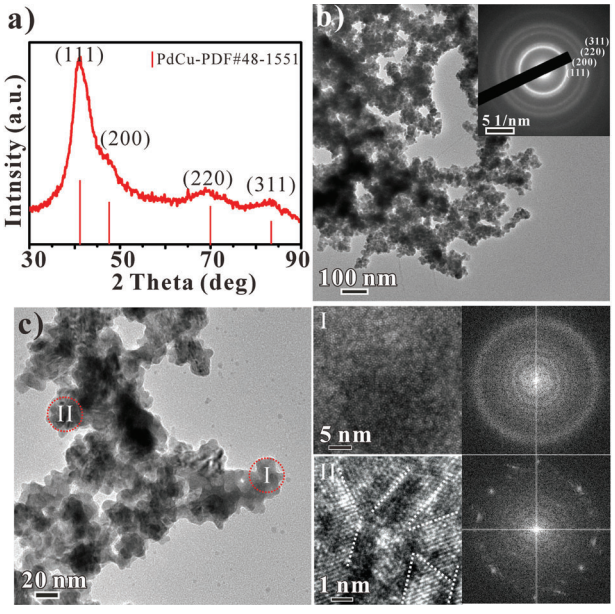

Figure 3. Typical structure features and morphology of the synthesized PdCu nanoalloys when adding 1.5 mmol $NaBH_4$ (10 mL aqueous) into 30 mL precursor solution dropwise. a) XRD pattern, b) TEM image at low magnification (inset: corresponding SAED pattern), and c) HRTEM images and FFT of different regions.

is lower than the critical supersaturation of the amorphous nuclei (low μ_l) all along, and these building blocks tend to assemble in a crystal pathway (low μ_s). However, more detailed structure information by HRTEM presents that there are still some areas with disordered arrangement (Figure 3c I) and the other crystal

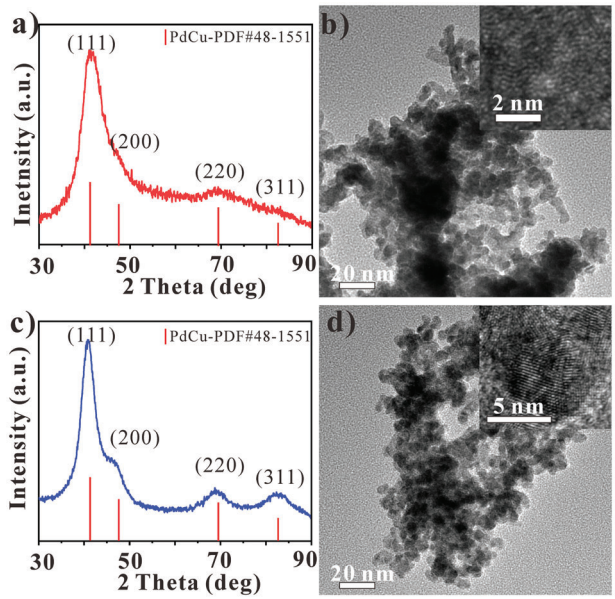

Figure 4. Typical structure features and morphology of the synthesized PdCu nanoalloys when adding an ultra-concentrated $NaBH_4$ droplet (0.3 mmol, 0.05 mL) into precursor solution. a) XRD pattern, b) TEM image at low magnification (inset: HRTEM image) of the PdCu nanoalloys synthesized without stirring; c) XRD pattern, d) TEM image at low magnification (inset: HRTEM image) of the PdCu nanoalloys synthesized with vigorous stirring.

regions are with abundant boundaries (Figure 3c II). The main reasons for the partial region with high energy (high μ_s) can be attributed to the fact that when every concentrated $NaBH_4$ droplet is dropped into the precursor solution, at the very beginning of the mixing between the droplet and the precursor solution, the metal ions around the interface can be reduced rapidly at this moment, then these local concentrated metal atoms aggregate fast and randomly to form amorphous structure superior than diffuse into the bulk to form a diluted solution. Therefore, this product is named as PdCu-amor/cryst.

2.1.3. Diffusion Control

As mentioned above, the diffusion rate of the reductant can also be a key point to affect the μ_s and further control the phase structure. In order to further verify this, in this third case, we added an ultra-concentrated droplet (0.3 mmol, 0.05 mL) into the precursor solution. As is shown in **Figure 4**a,b, when the $NaBH_4$ droplet was added into the precursor solution without stirring, the local metal atoms grew explosively under the ultrahigh μ_s condition, the amorphous phase dominated the final structure. While under much more vigorous stirring, the enhanced diffusion can efficiently and rapidly dilute the metal atoms, then the phase of the main products evolved to crystalline state in the growth condition with lower building block concentration (Figure 4c,d).

2.1.4. Universality

Importantly, the strategy of chemical-potential-controlled phase structure evolution can also be used to synthesize other Pd-based amorphous alloy. Such as amorphous PdFe, PdCo, and PdNi can also be successfully obtained by using concentrated reductant solution (**Figure 5**, Figure S4, Supporting Information), presenting a certain universality. As for these alloys, the appropriate mismatches of atom radius are 3.3% (PdFe), 3.7% (PdCu), 4.7% (PdCo), and 5.0% (PdNi), respectively. While for Pd-based alloy with smaller atom radius mismatch, like PdAg (2.4%), PdAu (2.3%), PdRh (1.1%), and PdPt (0.4%), they can hardly form metastable amorphous phase (Figure S5, Supporting Information). The mismatch-dependent phase structures can be explained as follows: with the larger mismatch, the metallic bond became looser, leading to the increase of defects, vacancies, and imperfections in the interior of alloy, destroying the long range periodic crystalline structure, tending to the formation of the metastable amorphous phase. In contrary, the smaller mismatch is beneficial to the tighter interatoms connection, the ordered structure can be further well sustained, resulting in the growth of crystalline phase.

2.2. Formic Acid Decomposition Performance

Pd-based nanomaterials have been under quite attention as efficient catalysts for generating green hydrogen source from formic acid (FA) decomposition. In recent decades, many efforts have been paid on studying the size effect, facet effects, as well as alloying effects,[13] while seldom attention was paid to the phase effects. What's more, thermodynamically, the redox potential of element Cu is more positive than that of H, while the ones of Fe, Co, and Ni are all more negative than that of H. It can be reasonably deduced that the PdCu alloy can present superior anticorrosion during FA decomposition to the other counterparts. Hence, in this paper, FA decomposition was further investigated to reveal the structure-activity effects on the synthesized PdCu nanostructures.

Figure 6 exhibits the hydrogen generation rate from FA decomposition for PdCu-cryst, PdCu-amor, and PdCu-amor/cryst with similar size and morphology. As is shown in Figure 6a, the hydrogen generation rate for PdCu-amor is up to 9.1×10^{-3} mL min^{-1} mg^{-1}_{Pd}, and can be well sustained above 8.3×10^{-3} mL min^{-1} mg^{-1}_{Pd} (just about 8.8% deactivation) after 2 h decomposition reaction. While for the PdCu-amor/cryst, the mass activity is decreased from 8.9×10^{-3} to 5.3×10^{-3} mL min^{-1} mg^{-1}_{Pd}, exhibiting 40% mass deactivation. The maximum mass activity (7.1×10^{-3} mL min^{-1} mg^{-1}_{Pd}) and the stability (presenting 65% mass deactivation after 2 h reaction (2.5×10^{-3} mL min^{-1} mg^{-1}_{Pd}) of the pure PdCu-cryst catalyst are even worse. As for the specific surface area activity, the decreasing trend is consistent with the ones of the mass activity, after 2 h reaction, the specific surface area activity of PdCu-amor decrease from 0.393 to 0.366 mL min^{-1} m^{-2}, while PdCu-amor/*fcc* is 0.424 to 0.282 mL min^{-1} m^{-2} and PdCu-*fcc* is 0.396 to 0.178 mL min^{-1} m^{-2} (Figure 6b). Based on the above results, it can be concluded that the presence of amorphous phase region of PdCu nanostructure can not only boost the catalytic activity but also enhance the catalytic stability. The superior catalytic performance of PdCu-amorphous can be resulted from below: first, benefit from the nature of amorphous phase, the active surface area of the amorphous one is about 14.4 m^2 g^{-1}, which is 1.11 fold larger than the amor/cryst

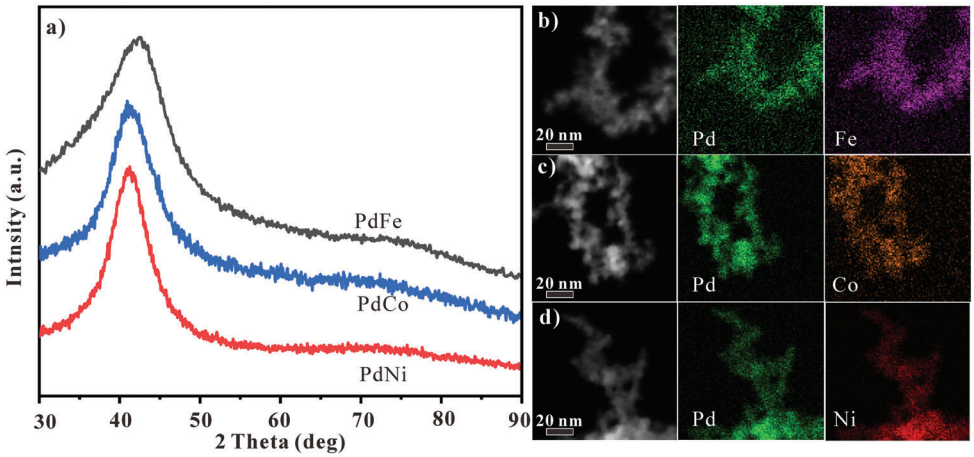

Figure 5. The structure features and morphology of Pd-based nanoalloys. a) PXRD patterns of amorphous PdFe, PdCo, and PdNi alloys. HAADF-STEM images and elements mapping images of b) PdFe, c) PdCo, and d) PdNi nanoalloys.

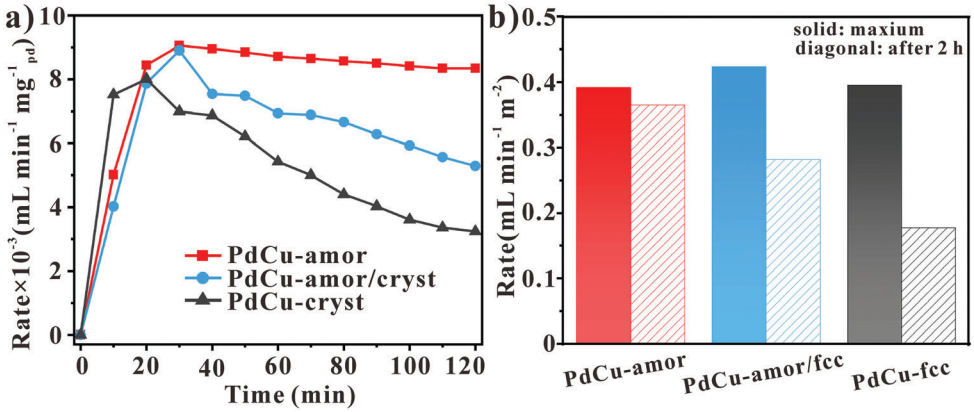

Figure 6. Hydrogen gas generation rate from FA aqueous solution detected by gas chromatography. a) Mass activity and b) specific surface area activity.

one (13.0 m^2 g^{-1}) and 1.14 fold larger than the crystalline one (12.6 m^2 g^{-1}) (Figure S6, Supporting Information), respectively; second, the high density of "dangling bonds" originated from the low-coordinated atom can act as active catalytic sites,[2] facilitating the decomposition of FA; third, it was reported that the lower electron density of Pd sites of PdCu-amor (Figure S7, Supporting Information) facilitates strengthening the H-Pd bond on the surface,[8a] which can benefit to the formation of HCOO* intermediates in the form of monodentate and/or bidentate formate species, promoting further decomposition reaction in the amorphous case. The in situ FTIR spectra on those nanostructures were also adopted to monitor the intermediates, which shows that no CO species but only FA species can be detected, indicating only the dehydrogenation pathway occurred during the decomposition reaction (Figure S8, Supporting Information). Besides, it is well known that corrosion usually occurs at domain boundaries, benefiting from the homogeneity in geometric configuration of the amorphous phase,[5a] the amorphous structure is free from the above feature and can undergo enhanced corrosion resistance during the FA decomposition reaction (Figure S9a–c, Supporting Information), while by comparison, the crystalline one with abundant edges and domain boundaries can hardly resist the corrosion during the FA decomposition reaction (Figure S9d–f, Supporting Information). Hence, the stability of the amorphous phase structure and the chemical compositions are the main reasons supporting the durability of the decomposition reaction.

3. Conclusion

In summary, based on the energy conservation between crystal growth units and newly formed solid phase in a nonequilibrium process, we propose the phase (amorphous or crystalline) of Pd-based nanostructures, such as PdFe, PdCo, PdNi, and PdCu, can be well controlled by varying the reduction conditions. Results, as we expected, illustrate that when grow in a solution with higher chemical potential, the obtained Pd-based nanoalloys prefer to present amorphous phase. In addition, the amorphous PdCu nanoalloys present superior catalytic activity and durability toward formic acid decomposition reaction. This effective and

universal strategy provides a new guidance in the rational design and synthesis of nanomaterials with metastable phase.

4. Experimental Section

Full details are provided in the Supporting Information.

Supporting Information

Supporting Information is available from the Wiley Online Library or from the author.

Acknowledgements

This work was supported by the National Key Research and Development Program of China (2020YFB1505802), the Natural Science Foundation of Xiamen, China (3502Z20227008), the National Natural Science Foundation of China (21931009 and 22275155), the Fundamental Research Funds for the Central Universities (20720210016, 20720210104, and 20720220136) and China Postdoctoral Science Foundation (2020M671939).

Conflict of Interest

The authors declare no conflict of interest.

Author Contributions

Q.J. conducted the synthesis and characterizations of the materials. Q.J. analyzed data and drafted the manuscript with the help of Y.D., L.L., Z.Z., and Z.-A.N.. J.Y. conducted the in situ FTIR spectra characterizations. Z.J. gave important advice during the experimental process. H.L. gave important advice on the data analysis and helped revise the manuscript. Z.X. proposed the research project and guided the whole experiment.

Data Availability Statement

The data that support the findings of this study are available in the supplementary material of this article.

Keywords

amorphous phase, chemical potential, formic acid decomposition, Pd-based nanoalloys, supersaturation

Received: November 17, 2022
Revised: January 12, 2023
Published online: March 12, 2023

[1] a) Z. Cao, Q. Chen, J. Zhang, H. Li, Y. Jiang, S. Shen, G. Fu, B. A. Lu, Z. Xie, L. Zheng, *Nat. Commun.* **2017**, *8*, 15131; b) Z. Fan, H. Zhang, *Chem. Soc. Rev.* **2016**, *45*, 63; c) X. Huang, S. Li, Y. Huang, S. Wu, X. Zhou, S. Li, C. L. Gan, F. Boey, C. A. Mirkin, H. Zhang, *Nat. Commun.* **2011**, *2*, 292.

[2] W. H. Wang, *Prog. Mater. Sci.* **2012**, *57*, 487.

[3] G. Wu, X. Zheng, P. Cui, H. Jiang, X. Wang, Y. Qu, W. Chen, Y. Lin, H. Li, X. Han, Y. Hu, P. Liu, Q. Zhang, J. Ge, Y. Yao, R. Sun, Y. Wu, L. Gu, X. Hong, Y. Li, *Nat. Commun.* **2019**, *10*, 4855.

[4] a) Y. Wu, Y. Xiao, G. Chen, C. T. Liu, Z. Lu, *Adv. Mater.* **2010**, *22*, 2770; b) W. H. Wang, R. J. Wang, F. Y. Li, D. Q. Zhao, M. X. Pan, *Appl. Phys. Lett.* **1999**, *74*, 1803; c) M. E. McHenry, M. A. Willard, D. E. Laughlin, *Prog. Mater. Sci.* **1999**, *44*, 291; d) J. F. Li, Y. Shao, X. Liu, K. F. Yao, *Sci. Bull.* **2015**, *60*, 396.

[5] a) J. R. Scully, A. Gebert, J. H. Payer, *J. Mater. Res.* **2011**, *22*, 302; b) X. Gu, Y. Zheng, S. Zhong, T. Xi, J. Wang, W. Wang, *Biomaterials* **2010**, *31*, 1093.

[6] a) J. Wang, L. Han, B. Huang, Q. Shao, H. L. Xin, X. Huang, *Nat. Commun.* **2019**, *10*, 5692; b) F. Hu, S. Zhu, S. Chen, Y. Li, L. Ma, T. Wu, Y. Zhang, C. Wang, C. Liu, X. Yang, L. Song, X. Yang, Y. Xiong, *Adv. Mater.* **2017**, *29*,160670; c) D. He, L. Zhang, D. He, G. Zhou, Y. Lin, Z. Deng, X. Hong, Y. Wu, C. Chen, Y. Li, *Nat. Commun.* **2016**, *7*, 12362; d) Q. Wang, L. Yun, M. Chen, D. Xu, Z. Cui, Q. Zeng, P. Lin, C. Chu, B. Shen, *ACS Appl. Nano Mater.* **2018**, *2*, 214; e) S. J. Li, D. Bao, M. M. Shi, B. R. Wulan, J. M. Yan, Q. Jiang, *Adv. Mater.* **2017**, *29*, 1700001; f) Y. Duan, Z. Y. Yu, S. J. Hu, X. S. Zheng, C. T. Zhang, H. H. Ding, B. C. Hu, Q. Q. Fu, Z. L. Yu, X. Zheng, J. F. Zhu, M. R. Gao, S. H. Yu, *Angew. Chem., Int. Ed.* **2019**, *58*, 15772.

[7] a) C. P. Royall, S. R. Williams, T. Ohtsuka, H. Tanaka, *Nat. Mater.* **2008**, *7*, 556; b) S. Manley, H. M. Wyss, K. Miyazaki, J. C. Conrad, V. Trappe, L. J. Kaufman, D. R. Reichman, D. A. Weitz, *Phys. Rev. Lett.* **2005**, *95*, 238302; c) S. M. Sharma, S. K. Sikka, *Prog. Mater. Sci.* **1996**, *40*, 1; d) O. Mishima, L. D. Calvert, E. Whalley, *Nature* **1984**, *310*, 393.

[8] a) N. Yang, H. Cheng, X. Liu, Q. Yun, Y. Chen, B. Li, B. Chen, Z. Zhang, X. Chen, Q. Lu, J. Huang, Y. Huang, Y. Zong, Y. Yang, L. Gu, H. Zhang, *Adv. Mater.* **2018**, *30*, 1803234; b) K. C. Poon, D. C. Tan, T. D. Vo, B. Khezri, H. Su, R. D. Webster, H. Sato, *J. Am. Chem. Soc.* **2014**, *136*, 5217.

[9] H. X. Lin, Z. C. Lei, Z. Y. Jiang, C. P. Hou, D. Y. Liu, M. M. Xu, Z. Q. Tian, Z. X. Xie, *J. Am. Chem. Soc.* **2013**, *135*, 9311.

[10] a) L. Zhang, W. Niu, W. Gao, L. Qi, J. Lai, J. Zhao, G. Xu, *ACS Nano* **2014**, *8*, 5953; b) W. Niu, Y. Duan, Z. Qing, H. Huang, X. Lu, *J. Am. Chem. Soc.* **2017**, *139*, 5817; c) Y. Jia, Y. Jiang, J. Zhang, L. Zhang, Q. Chen, Z. Xie, L. Zheng, *J. Am. Chem. Soc.* **2014**, *136*, 3748.

[11] J. Hong, J. H. Bae, H. Jo, H. Y. Park, S. Lee, S. J. Hong, H. Chun, M. K. Cho, J. Kim, J. Kim, Y. Son, H. Jin, J. Y. Suh, S. C. Kim, H. K. Roh, K. H. Lee, H. S. Kim, K. Y. Chung, C. W. Yoon, K. Lee, S. H. Kim, J. P. Ahn, H. Baik, G. H. Kim, B. Han, S. Jin, T. Hyeon, J. Park, C. Y. Son, Y. Yang, et al., *Nature* **2022**, *603*, 631.

[12] J. Zhang, G. Du, H. Li, Q. Chen, Q. Kuang, Z. Jiang, Z. Xie, *Small Methods* **2021**, *5*, 2000447.

[13] a) X. Zhou, Y. Huang, W. Xing, C. Liu, J. Liao, T. Lu, *Chem. Commun.* **2008**, 3540; b) D. Yuan, Y. Zhang, *Appl. Surf. Sci.* **2018**, *462*, 649; c) K. Jiang, K. Xu, S. Zou, W. B. Cai, *J. Am. Chem. Soc.* **2014**, *136*, 4861.